

Controlled Incorporation of Silver Nanoparticles into Layer-by-Layer Polymer Films for Reusable Electronic Tongues

Rafael C Hensel, Maria L Braunger, Bruno Oliveira, Flavio M Shimizu, Osvaldo N Oliveira, Matthias Hillenkamp, Antonio Riul, Varlei Rodrigues

▶ **To cite this version:**

Rafael C Hensel, Maria L Braunger, Bruno Oliveira, Flavio M Shimizu, Osvaldo N Oliveira, et al.. Controlled Incorporation of Silver Nanoparticles into Layer-by-Layer Polymer Films for Reusable Electronic Tongues. ACS Applied Nano Materials, 2021, 4 (12), pp.14231-14240. 10.1021/acsanm.1c03797 . hal-03526836

HAL Id: hal-03526836
https://hal.science/hal-03526836

Submitted on 14 Jan 2022

HAL is a multi-disciplinary open access archive for the deposit and dissemination of scientific research documents, whether they are published or not. The documents may come from teaching and research institutions in France or abroad, or from public or private research centers.

L'archive ouverte pluridisciplinaire **HAL**, est destinée au dépôt et à la diffusion de documents scientifiques de niveau recherche, publiés ou non, émanant des établissements d'enseignement et de recherche français ou étrangers, des laboratoires publics ou privés.

Controlled incorporation of silver nanoparticles into layer-by-layer polymer films for reusable electronic tongues

Rafael C. Hensel,[†] Maria L. Braunger,[†] Bruno Oliveira,[†] Flavio M. Shimizu,[†] Osvaldo N. Oliveira Jr.,[‡] Matthias Hillenkamp,[¶,†] Antonio Riul Jr.,[†] and Varlei Rodrigues[*,†]

†*Department of Applied Physics, "Gleb Wataghin" Institute of Physics (IFGW), University of Campinas (UNICAMP), Campinas, SP 13083-859, Brazil*

‡*São Carlos Institute of Physics, University of São Paulo, P.O Box 369, 13560-970 São Carlos, SP, Brazil*

¶*Institute of Light and Matter, University of Lyon, University Claude Bernard Lyon 1, CNRS, UMR5306, F-69622 Villeurbanne, France.*

E-mail: varlei@ifi.unicamp.br

Abstract

The incorporation of metallic nanoparticles in sensors and biosensors normally enhances performance, but fabricating reproducible sensing units is still an issue owing to the poor control of their electrical properties. In this article, we exploit the controlled deposition of silver nanoparticles (NP) pre-formed in a gas phase into layer-by-layer (LbL) films of poly(allylamine hydrochloride) (PAH) and poly(sodium 4-styrenesulfonate) (PSS) (PAH/PSS) assembled on gold interdigitated electrodes (IDEs). *In-situ* impedance measurements during NP deposition permitted the monitoring of the electrical response evolution, and reproducible sensing units could be made with tailored characteristics by varying the deposition time. In proof-of-principle experiments we employed an array with 4 sensing units in an electronic tongue (e-tongue), which was capable of distinguishing basic flavors of the human palate and diverse commercial umami-based flavor enhancer. Using statistical analysis methods it was possible to identify ways to optimize the e-tongue performance, thus confirming the possibility to explore controlled changes in electrical response via nanoparticle incorporation. It is worth noting that the methodology can be extended to produce other polymer-metallic NP composites and modify the electrical behavior of films in a controlled, reproducible manner, opening the way for enhanced opto-electronic devices, not limited to sensors or biosensors.

Introduction

The development of sensors for efficient, rapid, and reliable detection of analytes in volatile compounds or complex liquids is a global demand for environmental, agricultural, and food monitoring. A promising approach to the fabrication of sensing devices is to exploit nanostructured polymers as active layers to tune physicochemical properties with high precision,[1] and/or dope the polymer matrix to enhance sensing performance. For instance, the incorporation of metallic aggregates in polymeric matrices enhances sensing via the optical and electrical response due to the high surface-to-volume ratio of nanoparticles.[2] By

way of illustration, functionalization of glassy carbon electrodes with ferrocene terminated poly(amidoamine) dendrimers encapsulated with gold nanoparticles promoted high sensitivity and stability in detecting 4-aminophenol,[3] and cobalt phthalocyanine films modified with palladium and gold nanoparticles improved the performance of chemiresistive sensors for hydrogen.[4] In these examples, the enhancement mechanism can be related to the functional groups of the coating, to an increase in the surface area, modifications of the conductive path and geometric parameters.[2,5] Incorporation of metallic nanoparticles in sensors can enhance their specificity,[6] sensitivity,[7] and selectivity,[8–12] but an independent control of the nanoparticle synthesis and deposition to fine-tune the device response is still a technological bottleneck. With wet chemistry one may synthesize nanoparticles protected with functional groups that interact specifically with the analyte to increase selectivity,[13] and the thickness of the functional layer can be adjusted to favor the nanoparticle spatial ordering.[14] The synthesis and deposition of nanoparticles may also be carried out with atomic deposition of evaporated and/or sputtered metallic particles.[13] However, this method is limited since the wettability and mobility of atoms on the surface promote coalescence of the nanoparticles,[15–19] making it difficult to control their size and spatial distribution. To overcome these limitations one can deposit nanoparticles produced in the gas phase.[20,21] In this method, atoms sputtered from a metallic target[21] aggregate in an inert gas atmosphere under defined pressure and temperature. Then the pre-formed nanoparticles can be deposited at a defined kinetic energy to maintain their structure. The advantage of this technique is in the control of nanoparticle size, maintaining the nanoparticle interface free from surfactants. The fundamental differences between sputtered and passivated chemically synthesized nanoparticles are significant since plasmonic properties, chemical reactivity, catalytic activity, and electrical conduction critically depend on the particle-environment interface.

Here we explored the versatility of gas-phase generated nanoparticles to adjust in a controlled way the electrical response of a layer-by-layer film of poly(allylamine hydrochloride (PAH) and poly(sodium 4-styrene sulfonate) (PSS). In addition to the independent control

over the nanoparticle composition and size, as the deposition is performed in vacuum, the nanoparticles are free from surfactants and passivation layers. The electrical behavior of PAH/PSS films on interdigitated electrodes (IDEs) was monitored during the deposition of silver nanoparticles by impedance measurements. This method allowed us to tune the electrical behavior of PAH/PSS films with high reproducibility according to device impedance, and employ them in sensing units for an electronic tongue (e-tongue). Many types of materials have been used in nanostructured films for e-tongues,[22–25] which are based on the global selectivity principle,[26,27] according to which the electrical responses of an array of sensing units are combined to establish a "fingerprint" of the liquid under analysis. For some applications of e-tongues, however, the choice of materials and sensing units must be judicious to permit them to be reused. The two most stringent requirements for reuse are reproducibility of the electrical response and robustness against contamination. We show here that sensing units made with nanoparticle-containing PAH/PSS films fulfill these requirements in proof-of-principle experiments with e-tongues capable of distinguishing the basic tastes and different food samples with umami taste.

Methodology

Polymeric thin films

Gold IDEs on glass with 30 pairs of digits with 3 mm length, 200 nm height, 40 μm width, and spaced 40 μm from each other, were fabricated at the National Center for Research in Energy and Materials (CNPEM) Brazil. To favor adsorption of the polymer film on the IDE, we executed a cleaning procedure using a solution of hydrogen peroxide, ammonium hydroxide, and deionized water in the proportion (1:1:5). The IDE stood immersed for 10 min at a fixed temperature around 80°C. The polymeric thin films were deposited onto IDEs using the layer-by-layer (LbL) method[28,29] with alternating layers of PAH and PSS purchased from Sigma-Aldrich and used as received. The PAH and PSS solutions had 0.5

mg/mL in deionized water acquired from an Arium Comfort Sartorius system, whose pH was adjusted to 7. The LbL films were fabricated using a homemade automated setup, descried elsewhere.[30] We set the immersion time for both PSS and PAH to 8 min, with a 10 mm/min withdrawal speed. Although PAH and PSS are polyelectrolytes, the electrostatic interactions during the multilayer assemble promotes the formation of electrical dipoles, which confer an insulating behavior for the PAH/PSS LbL architecture.[31]

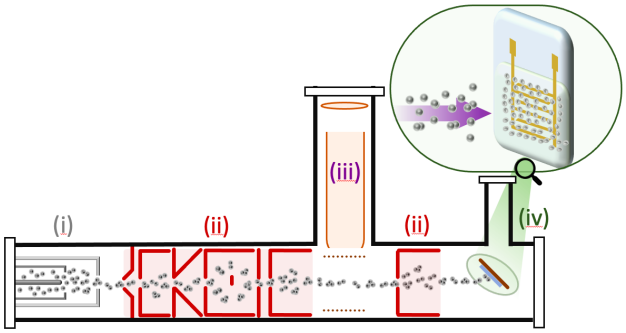


Figure 1: Schematic illustration of the experimental setup. Atomic cluster source used to produce and deposit the silver nanoparticles in the LbL film: (i) magnetron sputtering; (ii) set of electrostatic lens; (iii) time of flight mass spectrometer (TOF-MS); (iv) deposition chamber.

Nanoparticle production and deposition

Nanoparticles were produced in the gas phase using a gas-aggregation source shown in Figure 1.[32] Metal atoms are sputtered from a wire target. In a buffer gas (He/Ar), the atomic collisions and quenching cause nanoparticle formation (Figure 1(i)). A major fraction of the nanoparticles is positively charged and is guided through vacuum by a set of electrostatic lenses (Figure 1(ii)). Neutral nanoparticles are removed from the beam using a barrier. To monitor the nanoparticle size during deposition, a small fraction of the charged nanoparticles is deflected towards a TOF-MS, indicated in Figure 1(iii). The main nanoparticle beam is guided to the sample holder, where deposition occurs (Figure 1(iv)). The nanoparticle flux is monitored with a Keithley Series 6487 Picoammeter. We deposited silver nanoparticles of average diameter of 3 nm, with a typical current of 300-500 pA measured on the current

detector with 75 mm^2 area. The IDE electrical response was monitored during the silver nanoparticle deposition *in situ* using a homemade impedance meter, described in detail elsewhere.[33] Briefly, a sinusoidal voltage of 1 V amplitude an 1 kHz is applied to one comb of the IDE digits. The current from the pick-up electrode is amplified using an operational amplifier in a differential configuration.[30] A lock-in system measures the output voltage and the phase shift between the input and output signals. We interpreted the impedance measurements using an equivalent circuit coupling parallel capacitive and conductive components.[30]

Impedance spectroscopy

The electrical response of the IDEs in distilled water was evaluated using an impedance analyzer Solartron 1260A coupled to a dielectric interface model 1296A. The input voltage amplitude was set to 25 mV, with impedance measurements taken in the frequency range 1 Hz - 10^6 Hz, and interpreted using an equivalent electrical circuit of resistors and capacitors. We repeated this measurement after the PAH/PSS film assembly, and then nanoparticle deposition.

Morphological investigation

Two LbL films were prepared with different concentrations of silver nanoparticles incorporated in the PAH/PSS to investigate the depth profile of the silver nanoparticles in the polymer matrix. Using a Dual Beam Helios 660 from the CNPEM, we produced sample cross-section lamellae with the lift-off method[34] which were analyzed using Scanning Transmission Electron Microscopy with a High Angle Annular Dark Field (STEM-HAADF) detector in a JEOL 2100F operated at 200 kV, also from CNPEM.

E-tongue measurements

In proof-of-principle experiments, we employed an impedimetric electronic tongue (e-tongue) comprising sensing units of IDEs coated with PAH/PSS films with incorporated nanoparticles. The combination of several sensing units in an e-tongue aims at obtaining distinct electrical behaviors to provide a unique fingerprint of the samples.[35] To achieve this, we defined a procedure similar to the one reported by Garçon *et al*, in which they varied the proportion of two building blocks to differentiate the sensing units.[36] We used one bare IDE and three IDEs covered with 150-bilayer (PAH/PSS) LbL films, two of which had different concentrations of deposited silver nanoparticles. From here on, the sensing units will be referred to as follows: IDE 1 is the bare IDE, IDE 2 is covered by 150 PAH/PSS bilayers, IDEs 3 and 4 were the coated with 150-bilayer PAH/PSS LbL films with a lower and a higher concentration of silver nanoparticles, respectively. We chose silver nanoparticles for the efficient and easy production control in the atomic cluster source. The e-tongue performance was evaluated in basic tastes relevant to the human palate. We prepared 1 mM aqueous solutions of caffeine ($C_8H_{10}N_4O_2$), sucrose ($C_{12}H_{22}O_{11}$), sodium chloride (NaCl), hydrochloric acid (HCl), and L-glutamic acid ($C_5H_9NO_4$), corresponding respectively to bitter, sweet, salty, sour, and umami tastes. The measurements were performed in triplicate using a Solartron 1260A coupled to a dielectric interface model 1296A in the same configuration described before. The analysis were performed by immersing each IDE in a Becker containing the analyte solution in the following order: sucrose, caffeine, L-glutamic acid, NaCl, and HCl. We verified all sensing units in water after measuring each analyte sample to check possible cross-contamination caused by the analytes in the sensing units.

As a further test of the sensor selectivity, we analyzed samples that give umami flavor to food. These samples were provided by the Food Ingredients Division of Ajinomoto in Brazil, comprising monosodium glutamate (Aji-no-moto®), disodium inosinate (Ajitide IMP®), disodium inosinate + disodium guanylate in 1:1 ratio (Ajitide I+G®), and a yeast extract with umami flavor (Savorboost U®), in addition to a commercial monosodium

glutamate sample purchased in the United States of America (Accent®). Except for Savorboost U®, the chemical formulas of these umami samples differ from each other by a few atoms: Aji-no-moto® ($C_5H_8NNaO_4$), Ajitide IMP® ($C_{10}H_11N_4Na_2O_8P$), Ajitide I+G® ($C_{10}H_11N_4Na_2O_8P + C_{10}H_12N_5Na_2O_8P$). In addition, Aji-no-moto® and Accent® are composed of monosodium glutamate provided by different manufacturer. All measurements were compared to L-glutamic acid, with 2 mg of each analyte dispersed in 1 mL distilled water. The measurements were also performed by immersing the IDEs in each analyte solution in the following order: Aji-no-moto®, Accent®, L-glutamic acid, Ajitide IMP®, Ajitide I+G®, and Savorboost U®, also cross-checking the measurement in water after each analyte analysis.

Results and discussion

Electrical characterization

The controlled incorporation of silver nanoparticles in the PAH/PSS films was evaluated with *in-situ* impedance measurements performed at 1 kHz. Figure 2 shows that IDE 3 and IDE 4 had an impedance $8 \times 10^8\,\Omega$ before the nanoparticle incorporation started, indicating the insulating behavior of the polymer matrix. The impedance of these electrodes decreased only slightly during the first 0.6 h deposition at a rate of $-0.6 \times 10^8\,\Omega$/h, after which it dropped considerably. When nanoparticle incorporation was interrupted for IDE 3, after 1.4 h of deposition ($\sim$ 0.7 AgNP monolayer), its impedance stabilized at $1.0 \times 10^8\,\Omega$. Incorporation continued for IDE 4 until almost two hours ($\sim$ 0.9 AgNP monolayer), which caused the impedance to decrease further and stabilize at $1.2 \times 10^7\,\Omega$. It is worth noting that the impedance response is nearly identical for IDE 3 and IDE 4 before stopping deposition on IDE 3. Overall, in addition to indicating that the sensing units can be differentiated according to their impedance, the reproducibility of nanoparticle incorporation (Figure S1 in the Supporting Information) permits to fabricate devices with an adjustable electrical

response.

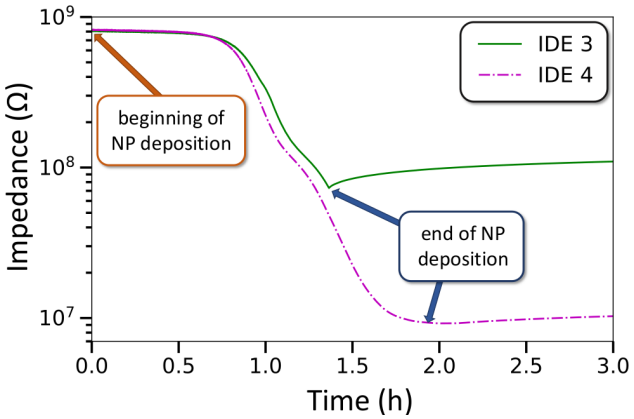


Figure 2: Impedance measurement at 1 kHz as a function of time of incorporation of silver nanoparticles for IDE 3 and IDE 4, with dashed lines marking the interruption of the incorporation. IDE 3 and IDE 4 had 150-bilayer PAH/PSS LbL films.

The electrical properties of the four sensing units with IDEs described in the methodology were assessed through impedance measurements in distilled water. The Nyquist plot in Figure 3(a) shows a semicircle corresponding to 10 kΩ followed by a diffusion process for the bare electrode (IDE 1). The deposition of a PAH/PSS LbL film onto IDE 2 caused the emergence of a second semicircle, the diameter of which further increased with the concentration of deposited silver nanoparticles (IDE 3 and IDE 4). A semicircle in a Nyquist plot is associated with a parallel coupling of capacitive and resistive components. To investigate the changes in electrical properties due to surface modification, the impedance data were interpreted using equivalent circuits[37] with the ZView software.[38] The fitted curves according to the equivalent circuits are also plotted as solid lines in Figure 3(a). The circuit that best represented the data for IDE 1 is shown in Figure 3(b), where R_{dl} and C_{dl} are the double-layer resistance and capacitance, respectively, R is the resistance after the double-layer formation which hinders charge mobility, CPE is the constant phase element assigned to an imperfect capacitance that is due to surface roughness and imperfections, and C_g is the geometric capacitance.[37] With deposition of a LbL film on electrodes IDE 2, IDE 3, and IDE 4 and incorporation of silver nanoparticles (IDE 3, and IDE 4), the equivalent circuit had to be extended to consider the contribution of the deposited materials onto the IDEs. The parallel

association of R_f and C_f represents the resistance and capacitance of the deposited material, respectively, as shown in Figure 3(c). CPE in the circuit of Figure 3(c) takes into account the surface imperfections due to adsorption of the film and silver nanoparticles deposition. The parameters used to fit the data with the equivalent circuits are given in Table 1, with high-quality fitting indicating by a χ^2 of the order of 10^{-5}. At low frequencies (< 100 Hz) the electric signal is dominated by double-layer effects, and the resistance R_{dl} increases from 184 to 214 kΩ due to the insulating LbL film, which then decreased to 61 and 56 kΩ with the increase of the deposited silver nanoparticles. The nanoparticle deposition causes the double layer capacitance to decrease owing to a reduction on the space between the "plates" of C_{dl}. The Bode plot in Figure 3 (d) indicates that the low frequency impedance decreases due to the polymer matrix and nanoparticles, which can be associated with ion accumulation on the device interface with the double-layer effects. At intermediate frequencies, dominated by the interfacial film/electrolyte response, the film resistance decreases with the nanoparticle deposition. This is attributed to creation of conducting paths in the (PAH/PSS) matrix.[2] The film capacitance increases with the nanoparticle deposition and their agglomeration in the polymer matrix. The extreme case here is the formation of a metallic nanoparticle film that is equivalent to introducing a new capacitor plate that reduces the gap between the capacitor plates. In the same frequency range, R and CPE increased with deposition of the LbL films and increasing incorporation of nanoparticles, which is explained by the decrease of the n factor,[37] thus suggesting a transition, of the whole system, from a capacitance to a resistance behavior. The Bode plots in Figure 3 (d) corroborate these interpretations, with an impedance increase in the intermediary frequency range (10^2 Hz and 10^4 Hz), where the electrical response is dominated by the film/electrolyte interface[39]. The dark arrow is a guide to the eye to illustrate the impedance increase in this frequency range. Note that the impedance at 1 kHz in Figure 2 decreases with the nanoparticle deposition, in contrast to the result in Figure 3 (d) because the measurements were performed in distinct media, i.e. vacuum (Figure 2) and distilled water (Figure 3 (d)). At higher frequencies (> 100 kHz),

the response is dominated by the geometry of the electrodes, which is constant, i.e., $C_g \approx$ 74 pF.

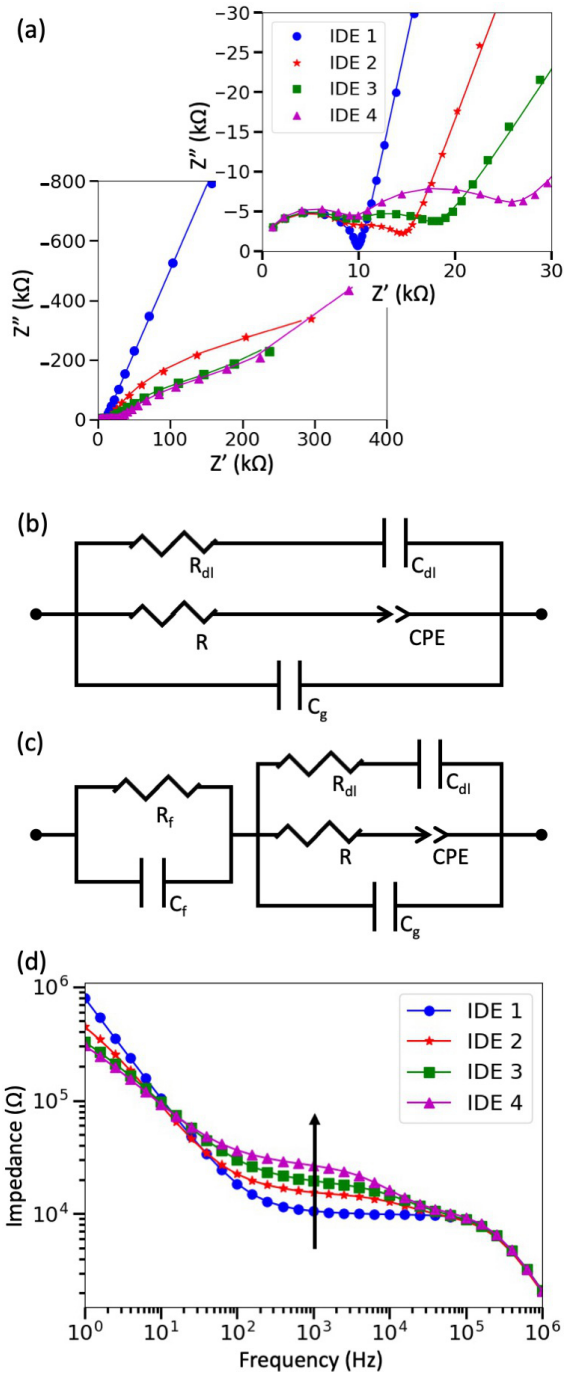


Figure 3: (a) Nyquist plots of IDEs 1-4 in distilled water. The solid lines indicate the fit using equivalent circuit evaluation. Scheme of the equivalent circuit used to evaluate (b) IDE 1, (c) IDE 2, IDE 3, and IDE 4. (d) Bode plots of the IDEs 1-4 in water. The black arrow is a guide to the eye to illustrate the impedance increase of the distinct sensing units.

Table 1: Fitting values for the equivalent circuit elements used to simulate the impedance spectra in Figure 3

IDEs	R_{dl} (kΩ)	C_{dl}(μF)	R_f (kΩ)	C_f(nF)	R (kΩ)	CPE(μF)	n	C_g(pF)
IDE 1	184±9	0.54±0.06	-	-	10.33 ± 0.01	0.24±0.01	0.89±0.01	73.35 ± 0.01
IDE 2	214±7	0.45±0.01	29.2±0.3	0.259 ± 0.006	14.33 ± 0.04	1.03±0.03	0.71±0.01	75.9 ± 0.3
IDE 3	61±2	0.66±0.02	24.4±0.3	0.274 ± 0.005	16.77 ± 0.07	1.23±0.02	0.61±0.02	72.7 ± 0.3
IDE 4	56±5	0.98±0.06	19.6±0.2	0.50 ± 0.01	24.0 ± 0.2	1.43±0.03	0.58±0.01	74.3 ± 0.6

Nanoparticle depth profile

The depth profile for the nanoparticles incorporated in the (PAH/PSS) polymer matrix was determined from the cross-section lamellae using STEM-HAADF. Figure 4 (a) and (b) show STEM-HAADF micrographs for samples with low and high silver nanoparticle concentrations, similar to IDE 3 and IDE 4, respectively. The sketch in Figure 4 (c) helps identify the sample cross-section layers. Carbon and platinum layers were deposited to reduce damages during ion beam milling on the polymeric film with nanoparticles. Bright spots due to the silver nanoparticles are seen below the carbon layer in Figures 4 (a) and (b). In both cases, the micrographs indicate that silver nanoparticles were deposited in the polymer matrix, and agglomerated in bigger structures near the polymer surface, especially for the high nanoparticle concentration. Although the micrographs do not have enough particles for a size distribution analysis, we measured their diameter in the direction perpendicular to the substrate (Figure 4), obtaining a mean diameter of 11 ± 6 nm and 19 ± 4 nm for lower and higher concentrations, respectively (Figure S2 in the Supporting Information). However, we must be careful in estimating the agglomeration size as TEM micrographs are projected images, so the measured diameter can be related to more than one projected structure due to the non-negligible lamellae thickness.

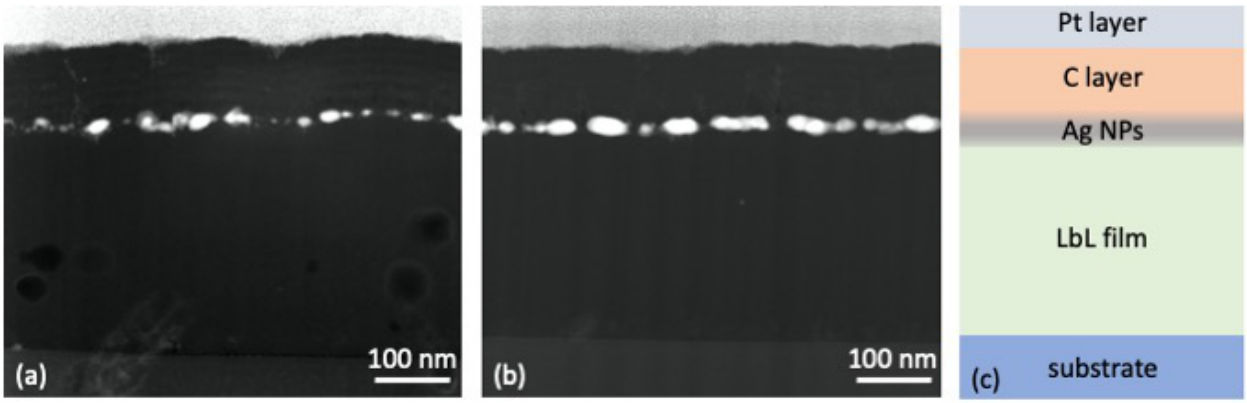


Figure 4: HAADF STEM micrographs of samples with nanoparticle concentrations similar to those of (a) IDE 3, and (b) IDE 4, respectively. (c) Sketch of the samples cross-section's tiers.

Impedimetric E-tongue

The control of electrical response imparted by incorporation of silver nanoparticles into LbL films was exploited in proof-of-principle experiments with an impedimetric e-tongue made with the four sensors in two tasks: to distinguish among the aqueous solutions representing the basic tastes and differentiate flavor enhancers with umami taste. We first demonstrate that a single sensing unit is already capable of some differentiation of the basic tastes, as indicated in the impedance spectra obtained with IDE 4 in Figure 5 (a). Indeed, in subsidiary statistical analyses we verified that full distinction of the basic tastes was possible with this sensing unit, as will be demonstrated later on. A similar finding was observed for the other three sensing units whose spectra are shown in Figures S2 in the Supporting Information. It is significant in the figure that the spectra for sucrose and caffeine are similar because they are weak electrolytes. Another important issue here is to investigate if the taste solutions change irreversibly the impedance response of the devices. Figure 5 (b) shows that the impedance spectra for IDE 4 in water is not affected by measurements in the basic taste solutions, which means there is no cross-contamination of the sensing unit. We repeated this procedure for IDEs 1-3, and there was no evidence of cross-contamination either, as shown in Figures S3 in the Supporting Information.

We applied principal component analysis (PCA)[40] over the whole impedance spectra to

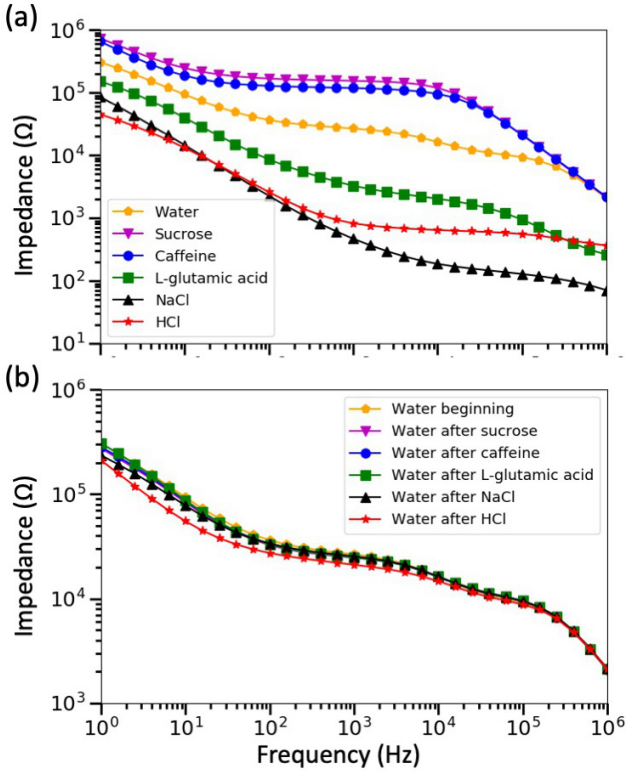


Figure 5: Impedance spectra for IDE 4: (a) in the aqueous solutions corresponding to the basic taste; (b) in water after measurement in the basic taste solutions.

investigate the capability of each sensing unit of the e-tongue for discriminating the basic flavor analytes. We used the open-source software Orange for data analysis and visualization,[41] which makes it possible to evaluate the number of clusters using the k-means method.[42] Briefly, k-means interactively defines the center of each cluster, minimizing the sum of square Euclidean distances between the center and its assigned data points. The quality of the cluster was compared using the silhouette plot, evaluating how close each point in one cluster is to points in the neighboring clusters. The silhouette value s(i) of the i^{th} cluster ranges between -1 and 1, with the following interpretation: (a) if s(i) $\sim$ 1 the object is well classified in a cluster; (b) if s(i) $\sim$ 0 the object lies between two clusters; (c) if s(i) $\sim$ -1 the object is badly classified. The maximum value for mean $\overline{S(k)}$ over all objects in the data set for k clusters provides the silhouette coefficient (SC), which varies between 0 and 1 having the following interpretation: (a) $0.71 < SC < 1.00$ corresponds to a strong distinction capability;

(b) $0.51 < SC < 0.70$ means a reasonable distinction capability; (c) $0.26 < SC < 0.50$ refers to a weak or artificial distinction capability; (d) SC $\leq$0.25 corresponds to no distinction capability at all.[43,44] Figure S5 in the Supporting Information shows that IDE 1, IDE 2, and IDE 3 can discriminate the basic tastes for the human palate. However, with IDE 4 the data for one caffeine sample is out of the expected cluster. The mean silhouette of each cluster for each sensing unit is shown in Table 2. From the SC values we infer that IDE 1 better distinguishes all analytes, with IDE 3 presenting the second highest SC value and better discrimination for strong electrolytes (HCl, L-glutamic acid, NaCl), with S(k)>0.91. This indicates that insertion of the nanoparticles into the polymer matrix increases the ability to identify electrolytes, possibly due to higher interacting area (from nanoparticles) with ions in solution. Surprisingly, IDE 4 exhibited lower SC compared to IDE 3, maybe because it poorly recognized caffeine triplicate. Our interpretation is that the high concentration of silver nanoparticles in IDE 4 was deleterious to the electrical response owing to nanoparticle clustering/compaction during the deposition process. That a single sensing unit could already provide full distinction of the samples is attributed to the combination of electrical responses from various frequencies, as different mechanisms govern the electrical response at distinct frequency regions. Hence, one sensing unit may play the role of an e-tongue if one considers that global selectivity is warranted by this combination of responses.

We also verified that combining the sensing units led to an increase in SC in Table S1 in the Supporting Information. As expected, a higher SC was obtained combining the impedance spectra of all sensing units. Results for the five basic tastes with the whole impedance frequency range for the four sensing units are shown in Figure 6, where each spectrum is represented by a marker. There are three markers for each analyte because the measurements were made in triplicate. Table 2 lists the mean silhouette value $\overline{s(i)}$ for each cluster i in the set of k clusters in Figures 6, with the highest silhouette coefficients (SC) obtained using the k-means method. $\overline{s(k)} = 0.88$ for a classification in k=5 clusters. According to Figure 6 and Table 2 the main difference in electrical response captured by the e-

tongue can be established with only the first principal component (PC1) that describes 99.0% of the data. Thus PC1 distinguishes electrolytes (HCl, NaCl, and L-glutamic acid, in the left-hand side) from non-electrolytes (caffeine and sucrose, in the right hand side). Although the second principal component (PC2) expresses only 0.5%, it is capable of distinguishing the three electrolyte samples, and the two non-electrolyte samples. It is worth noting that $\overline{s(i)} > 0.71$ in all cases owing to a strong distinction capability for the data in each cluster i. Of special relevance was the separation of the umami flavor (L-glutamic acid) in Figure 6, which is an achievement since this flavor is difficult to distinguish using e-tongues.[25,45]

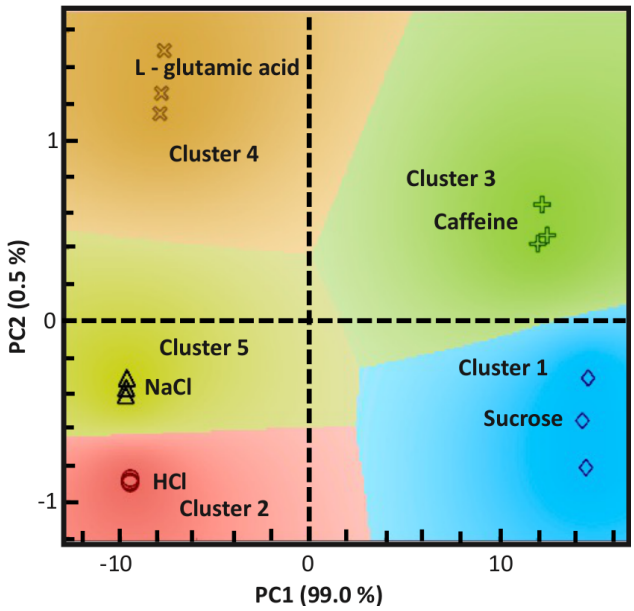


Figure 6: PCA plot with the impedance spectra obtained with the electronic tongue for the basic flavors: HCl (sour), L-glutamic acid (umami), NaCl (salt), caffeine (bitter), sucrose (sweet). The data set was separated into five clusters according to the maximum $\overline{S(k)}$ value that correctly distinguished the five samples.

The positive results for umami in the evaluation of the basic tastes motivated us to pursue it further in samples of food enhancers. This topic has deserved increasing attention owing to the difficulties with the umami flavor, for which e-tongues have been produced with various materials, including peptides, biotaste receptors and polymers with nanoparticles incorporated.[46–55] Figure S6 in the supporting information shows the impedance spectra for

Table 2: Mean silhouette value $\overline{s(i)}$ for the i^{th} cluster distinguished in the PCA plot of basic flavors using the whole frequency range for each IDE and the four sensing units.

IDEs	$\overline{s(1)}$	$\overline{s(2)}$	$\overline{s(3)}$	$\overline{s(4)}$	$\overline{s(5)}$	SC
IDE 1	0.89	0.89	0.88	0.85	0.91	$\overline{S(5)} = 0.88$
IDE 2	0.61	0.69	0.58	0.83	0.69	$\overline{S(5)} = 0.68$
IDE 3	0.55	0.92	0.76	0.94	0.95	$\overline{S(5)} = 0.82$
IDE 4	0.61	0.79	0.45	0.77	0.89	$\overline{S(5)} = 0.70$
All IDEs	0.85	0.94	0.82	0.88	0.91	$\overline{S(5)} = 0.88$

the umami-flavored food enhancer samples with the sensing units IDEs 1-4. Exposure to the food enhancers did not affect the electrical response of the sensing units, as indicated by the measurements in water in Figure S6 in the Supporting Information. The spectra are very similar to each other, in contrast to the basic flavor measurements, and distinction can only be done with a statistical analysis. The use of k-means associated with PCA allows the investigation of which sensing unit contributes most to sample distinction. The PCA plot using the whole impedance spectra for each IDE is shown in Figure S9 in the Supporting Information, while the silhouette values are given in Table 3. Full distinction of the six umami samples could be achieved using the data from a single sensing unit (IDE 2, IDE 3 or IDE 4), with IDE 3 presenting the higher SC. In contrast to the analysis of basic tastes, IDE 1 (bare electrode) was unable to provide good distinction, grouping two different brands of monosodium glutamate. Therefore, there should be an optimal NP density that maximizes the distinguishing capability of a sensing unit. We also obtained SC for each cluster by combining two, three and all four IDEs, as presented in Table S2 in the Supporting Information. The highest SC was obtained by combining IDE 2, IDE 3, and IDE 4, followed by the four IDEs together. The PCA plot using the four units is shown in Figure 7, where the mean silhouette value $\overline{s(i)}$ is higher than 0.71 for all clusters (see Table 3). Since both Ajitide IMP® and Ajitide I+G® contain disodium inosinate, they were positioned in the same region in the PC1 direction, and clearly distinguished by PC2. The latter was also useful to distinguish L-glutamic acid (also known as glutamate) from the two monosodium glutamates, i.e. Accent® and Aji-no-moto®, which were separated by PC1. The yeast extract was

clustered on the upper right-hand side. The distinction ability using the whole spectra could not be improved by applying feature selection, a common procedure in information visualization. We have tested this by applying the parallel coordinates technique[56] to identify the frequencies that most contribute to the classification of the samples, but the resulting PCA and interactive document mapping (IDMAP)[56] plots in Figure S10 and S11 in the Supporting Information were not improved in comparison to Figure 7.

The e-tongue results taken together are a demonstration that the controlled incorporation of nanoparticles in LbL polymer films allows for the reuse of sensing units with reproducible electrical responses. For umami, in particular, there was no need to functionalize the sensor surface with peptides. The high performance in distinguishing basic tastes and food enhancer samples with umami flavor may be exploited in monitoring other types of food and in agriculture,[57] which is important to replace panels of human experts with their inherent limitations due to toxicity of some compounds and personal subjectivity.[58]

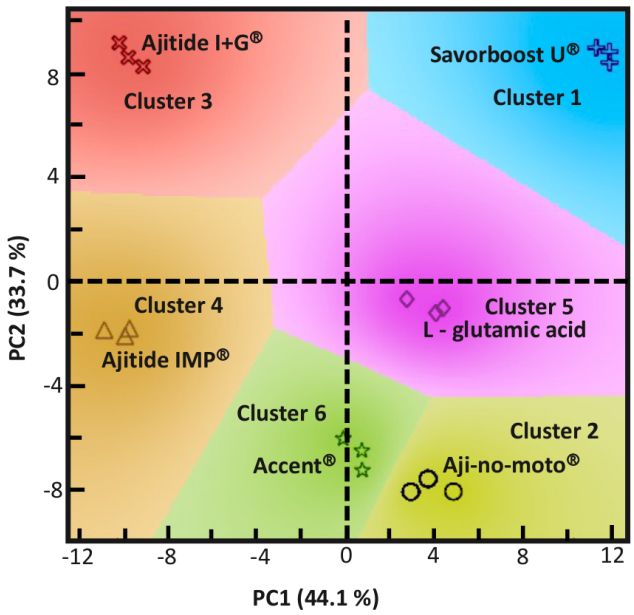


Figure 7: PCA plot obtained with the whole impedance spectra (between 10^0 Hz and 10^6 Hz) of the four sensing units of the e-tongue for the various samples having umami flavor.

Table 3: Mean silhouette values $\overline{s(i)}$ for the i^{th} cluster distinguished in PCA for umami flavor enhancer using the whole frequency range for each IDE and the four sensing units.

IDEs	$\overline{s(1)}$	$\overline{s(2)}$	$\overline{s(3)}$	$\overline{s(4)}$	$\overline{s(5)}$	$\overline{s(6)}$	$\overline{S(k)}$
IDE 1	0.79	0.46	0.84	0.74	0.46	-	$\overline{S(5)} = 0.66$
IDE 2	0.77	0.76	0.69	0.84	0.58	0.30	$\overline{S(6)} = 0.66$
IDE 3	0.90	0.51	0.97	0.67	0.65	0.54	$\overline{S(6)} = 0.71$
IDE 4	0.98	0.21	0.91	0.90	0.87	0.32	$\overline{S(6)} = 0.70$
All IDEs	0.92	0.75	0.86	0.92	0.76	0.74	$\overline{S(6)} = 0.83$

Conclusions

We explored the versatility of gas-phase produced nanoparticles to modify the electrical impedance of an insulating polymer matrix by controlling the nanoparticle deposition. Impedance measurements during the nanoparticle deposition allowed us to keep track of the electrical response of IDEs covered by PAH/PSS LbL films. We also demonstrated the reproducibility and stability of the device electrical response, which supports the development of reproducible sensing units - a bottleneck in the field of sensing and biosensing. The sensing units were applied in an e-tongue with proof-of-principle experiments to distinguish basic tastes relevant to human perception at low molar concentrations (1 mM) and different commercial food-enhancers having the umami taste presenting high reproducibility on triplicate analysis. The silhouette coefficient indicates better clustering in the presence of the nanoparticles for the umami analysis, which can also be interpreted as an increased discrimination performance. Briefly, the introduction of nanoparticles can be interpreted as the addition of new conducting pathways facilitating the electric transport and better electrode/electrolyte interaction. Our methodology to fabricate sensing units with defined impedance response opens new perspectives for monitoring food quality, in precision agriculture to evaluate nutrients in the soil and avoid over-fertilization, and the early diagnosis of many diseases. Moreover, the incorporation of nanoparticles can be extended to other types of metals and film-forming materials, thus permitting to envisage applications other than in sensing and biosensing.

Acknowledgement

The authors are grateful to FAPESP (2007/01722-9, 2014/03691-7, 2015/14836-9, 2016/12807-4, 2017/19169-6, 2018/22214-6), CNPq, and CAPES (Finance Code 001 - 1634666/2016) for financial support. Experimental support from the Microfabrication Laboratory (proposal LMF-18748 and LMF-21855) and Electron Microscopy Laboratory (proposal TEM-21702, ME-22308, TEM-23432, TEM-24315, TEM-C1-25093) at Brazilian Nanotechnology National Laboratory (LNNano), CNPEM, Campinas, Brazil for their support with the use of equipment.

Supporting Information Available

Dear co-authors,

The Supporting Information was submitted separately.

References

(1) Cichosz, S.; Masek, A.; Zaborski, M. Polymer-based sensors: A review. *Polymer Testing* **2018**, *67*, 342–348.

(2) Montes-García, V.; Squillaci, M. A.; Diez-Castellnou, M.; Ong, Q. K.; Stellacci, F.; Samorì, P. Chemical sensing with Au and Ag nanoparticles. *Chemical Society Reviews* **2021**, *50*, 1269–1304.

(3) Elancheziyan, M.; Senthilkumar, S. Redox-active gold nanoparticle-encapsulated poly(amidoamine) dendrimer for electrochemical sensing of 4-aminophenol. *Journal of Molecular Liquids* **2021**, *325*, 115131.

(4) Nikolaeva, N. S.; Klyamer, D. D.; Zharkov, S. M.; Tsygankova, A. R.; Sukhikh, A. S.; Morozova, N. B.; Basova, T. V. Heterostructures based on Pd–Au nanoparticles and

cobalt phthalocyanine for hydrogen chemiresistive sensors. *International Journal of Hydrogen Energy* **2021**, *46*, 19682–19692.

(5) Wang, F.; Hu, S. Electrochemical sensors based on metal and semiconductor nanoparticles. *Microchimica Acta* **2009**, *165*, 1–22.

(6) Soares, J. C.; Iwaki, L. E. O.; Soares, A. C.; Rodrigues, V. C.; Melendez, M. E.; Fregnani, J. H. T. G.; Reis, R. M.; Carvalho, A. L.; Corrêa, D. S.; Oliveira, O. N. Immunosensor for Pancreatic Cancer Based on Electrospun Nanofibers Coated with Carbon Nanotubes or Gold Nanoparticles. *ACS Omega* **2017**, *2*, 6975–6983.

(7) de Barros, A.; Constantino, C. J. L.; da Cruz, N. C.; Bortoleto, J. R. R.; Ferreira, M.; Barros, A. D.; José, C.; Constantino, L.; Cristino, N.; Roberto, J.; Bortoleto, R.; Ferreira, M. High performance of electrochemical sensors based on LbL films of gold nanoparticles, polyaniline and sodium montmorillonite clay mineral for simultaneous detection of metal ions. *Electrochimica Acta* **2017**, *235*, 700–708.

(8) Diouf, A.; Moufid, M.; Bouyahya, D.; Österlund, L.; El Bari, N.; Bouchikhi, B. An electrochemical sensor based on chitosan capped with gold nanoparticles combined with a voltammetric electronic tongue for quantitative aspirin detection in human physiological fluids and tablets. *Materials Science and Engineering: C* **2020**, *110*, 110665.

(9) Teodoro, K. B. R.; Shimizu, F. M.; Scagion, V. P.; Correa, D. S. Ternary nanocomposites based on cellulose nanowhiskers, silver nanoparticles and electrospun nanofibers: Use in an electronic tongue for heavy metal detection. *Sensors and Actuators B: Chemical* **2019**, *290*, 387–395.

(10) Garcia-Hernandez, C.; Medina-Plaza, C.; Garcia-Cabezon, C.; Blanco, Y.; Fernandez-Escudero, J. A.; Barajas-Tola, E.; Rodriguez-Perez, M. A.; Martin-Pedrosa, F.; Rodriguez-Mendez, M. L. Monitoring the Phenolic Ripening of Red Grapes Using a

406 Multisensor System Based on Metal-Oxide Nanoparticles. *Frontiers in Chemistry* **2018**,
407 *6*, 131.

408 (11) de Sá, A. C.; Cipri, A.; González-Calabuig, A.; Stradiotto, N. R.; del Valle, M. Res-
409 olution of galactose, glucose, xylose and mannose in sugarcane bagasse employing a
410 voltammetric electronic tongue formed by metals oxy-hydroxide/MWCNT modified
411 electrodes. *Sensors and Actuators B: Chemical* **2016**, *222*, 645–653.

412 (12) Mercante, L. A.; Scagion, V. P.; Pavinatto, A.; Sanfelice, R. C.; Mattoso, L. H. C.;
413 Correa, D. S. Electronic tongue based on nanostructured hybrid films of gold nanopar-
414 ticles and phthalocyanines for milk analysis. *Journal of Nanomaterials* **2015**, *2015*,
415 24275–24281.

416 (13) Prakash, S.; Chakrabarty, T.; Singh, A. K.; Shahi, V. K. Polymer thin films embedded
417 with metal nanoparticles for electrochemical biosensors applications. *Biosensors and*
418 *Bioelectronics* **2013**, *41*, 43–53.

419 (14) Lin, H.; Song, L.; Huang, Y.; Cheng, Q.; Yang, Y.; Guo, Z.; Su, F.; Chen, T.
420 Macroscopic Au@PANI Core/Shell Nanoparticle Superlattice Monolayer Film with
421 Dual-Responsive Plasmonic Switches. *ACS Applied Materials and Interfaces* **2020**, *12*,
422 11296–11304.

423 (15) Maréchal, N.; Quesnel, E.; Pauleau, Y. Silver thin films deposited by magnetron sput-
424 tering. *Thin Solid Films* **1994**, *241*, 34–38.

425 (16) Chan, K. Y.; Teo, B. S. Sputtering power and deposition pressure effects on the electrical
426 and structural properties of copper thin films. *Journal of Materials Science* **2005**, *40*,
427 5971–5981.

428 (17) Arnalds, U. B.; Agustsson, J. S.; Ingason, A. S.; Eriksson, A. K.; Gylfason, K. B.;
429 Gudmundsson, J. T.; Olafsson, S. A magnetron sputtering system for the preparation

of patterned thin films and in situ thin film electrical resistance measurements. *Review of Scientific Instruments* **2007**, *78*, 1–6.

(18) Novotny, M. In-situ monitoring of the growth of nanostructured aluminum thin film. *Journal of Nanophotonics* **2011**, *5*, 051503.

(19) Abdellaoui, N.; Pereira, A.; Novotny, M.; Bulir, J.; Fitl, P.; Lancok, J.; Moine, B.; Pillonnet, A. In situ monitoring of electrical resistance during deposition of Ag and Al thin films by pulsed laser deposition: Comparative study. *Applied Surface Science* **2017**, *418*, 517–521.

(20) Haberland, H.; Karrais, M.; Mall, M.; Thurner, Y. Thin films from energetic cluster impact: A feasibility study. *Journal of Vacuum Science & Technology A: Vacuum, Surfaces, and Films* **1992**, *10*, 3266–3271.

(21) Wegner, K.; Piseri, P.; Tafreshi, H. V.; Milani, P. Cluster beam deposition: a tool for nanoscale science and technology. *Journal of Physics D: Applied Physics* **2006**, *39*, R439–R459.

(22) Arrieta, A.; Rodriguez-Mendez, M. L.; de Saja, J. A. Langmuir–Blodgett film and carbon paste electrodes based on phthalocyanines as sensing units for taste. *Sensors and Actuators B: Chemical* **2003**, *95*, 357–365.

(23) Ferreira, M.; Riul Antonio,; Wohnrath, K.; Fonseca, F. J.; Oliveira Osvaldo N.,; Mattoso, L. H. C. High-Performance Taste Sensor Made from Langmuir-Blodgett Films of Conducting Polymers and a Ruthenium Complex. *Analytical Chemistry* **2003**, *75*, 953–955.

(24) Lvova, L.; Pudi, R.; Galloni, P.; Lippolis, V.; Di Natale, C.; Lundström, I.; Paolesse, R. Multi-transduction sensing films for Electronic Tongue applications. *Sensors and Actuators B: Chemical* **2015**, *207*, 1076–1086.

(25) Daikuzono, C. M.; Dantas, C. A.; Volpati, D.; Constantino, C. J.; Piazzetta, M. H.; Gobbi, A. L.; Taylor, D. M.; Oliveira, O. N.; Riul, A. Microfluidic electronic tongue. *Sensors and Actuators, B: Chemical* **2015**, *207*, 1129–1135.

(26) Toko, K. Taste sensor with global selectivity. *Materials Science and Engineering: C* **1996**, *4*, 69–82.

(27) Toko, K. Taste sensor. *Sensors and Actuators B: Chemical* **2000**, *64*, 205–215.

(28) Decher, G.; Hong, J.; Schmitt, J. Buildup of ultrathin multilayer films by a self-assembly process: III. Consecutively alternating adsorption of anionic and cationic polyelectrolytes on charged surfaces. *Thin Solid Films* **1992**, *210-211*, 831–835.

(29) Decher, G. *Multilayer Thin Films*; Wiley Online Books; 2012; pp 1–21.

(30) Hensel, R. C.; Rodrigues, K. L.; Pimentel, V. D. L.; Riul, A.; Rodrigues, V. Automated self-assembly and electrical characterization of nanostructured films. *MRS Communications* **2018**, *8*, 283–288.

(31) Hensel, R. C.; Pereira-da Silva, M. A.; Riul, A.; Rodrigues, V. Dielectric Permittivity and Surface Charge Density in Layer-by-Layer Poly(diallyldimethylammonium chloride)/Poly(styrenesulfonate) Nanostructured Films: Implications for Biosensing. *ACS Applied Nano Materials* **2020**, *3*, 1749–1754.

(32) de Sá, A. D. T.; Abrao Oiko, V. T.; di Domenicantonio, G.; Rodrigues, V. New experimental setup for metallic clusters production based on hollow cylindrical magnetron sputtering. *Journal of Vacuum Science & Technology B, Nanotechnology and Microelectronics: Materials, Processing, Measurement, and Phenomena* **2014**, *32*, 061804.

(33) Hensel, R. C.; Gonçalves, M. H.; Rodrigues, K. L.; A. Oiko, V. T.; do L. Pimentel, V.; Pereira-da Silva, M. A.; Hillenkamp, M.; Riul Jr., A.; Rodrigues, V. Monitoring and

modeling the deposition of metal nanoparticles on surfaces by impedance. *Applied Surface Science* **2020**, 148806.

(34) Rivera, F.; Davis, R.; Vanfleet, R. Alternative FIB TEM sample preparation method for cross-sections of thin metal films deposited on polymer substrates. *Microscopy and Microanalysis* **2013**, *19*, 1080–1091.

(35) Shimizu, F. M.; Braunger, M. L.; Riul Jr., A.; Oliveira Jr., O. N. Electronic Tongues. 2020; https://doi.org/10.1002/9781119587422.ch4.

(36) Garçon, L. A.; Genua, M.; Hou, Y.; Buhot, A.; Calemczuk, R.; Livache, T.; Billon, M.; Narvor, C. L.; Bonnaffé, D.; Lortat-Jacob, H.; Hou, Y. A versatile electronic tongue based on surface plasmon resonance imaging and cross-reactive sensor arrays—a minireview. *Sensors (Switzerland)* **2017**, *17*, 1–12.

(37) Taylor, D.; Macdonald, A. AC admittance of the metal/insulator/electrolyte interface. *Journal of Physics D: Applied Physics* **1987**, *20*, 1277.

(38) Inc., S. A. ZView® For Windows. 2017; https://www.scribner.com/software/68-general-electrochemistr376-zview-for-windows/.

(39) Macdonald, J. R.; Barsoukov, E. Impedance spectroscopy: theory, experiment, and applications. *History* **2005**, *1*, 1–13.

(40) Davies, H. M.; Hope, K. Methods of Multivariate Analysis. *The Mathematical Gazette* **1972**, *56*.

(41) Orange Website. 2019; www.orange.com, visited on 2020-11-11.

(42) Hartigan, J. A.; Wong, M. A. A K-Means Clustering Algorithm. *Journal of the Royal Statistical Society: Series C (Applied Statistics)* **1979**, *28*, 100–108.

(43) Kaufman, L.; Rousseeuw, P. J. *Eepe.Ethz.Ch*; 1990.

(44) Struyf, A.; Hubert, M.; Rousseeuw, P. Clustering in an Object-Oriented Environment. *Journal of Statistical Software, Articles* **1997**, *1*, 1–30.

(45) Braunger, M. L.; Fier, I.; Rodrigues, V.; Arratia, P. E.; Riul, A. Microfluidic Mixer with Automated Electrode Switching for Sensing Applications. *Chemosensors* **2020**, *8*, 13.

(46) Yang, Y.; Chen, Q.; Shen, C.; Zhang, S.; Gan, Z.; Hu, R.; Zhao, J.; Ni, Y. Evaluation of monosodium glutamate, disodium inosinate and guanylate umami taste by an electronic tongue. *Journal of Food Engineering* **2013**, *116*, 627–632.

(47) Feng, T.; Bing, F.; Yang, Y.; Zhuang, H.; Ye, R.; Li, X.; Xu, Z.; Wang, K. Discrimination of edible fungi varieties and evaluation of their umami intensities by using an electronic tongue method. *International Journal of Food Science & Technology* **2016**, *51*, 1393–1400.

(48) Phat, C.; Moon, B.; Lee, C. Evaluation of umami taste in mushroom extracts by chemical analysis, sensory evaluation, and an electronic tongue system. *Food Chemistry* **2016**, *192*, 1068–1077.

(49) Mondal, D.; Paul, D.; Mukherji, S. Conducting polymer coated filter paper based disposable electronic tongue. 2018 12th International Conference on Sensing Technology (ICST). 2018; pp 7–12.

(50) Ahn, S. R.; An, J. H.; Jang, I. H.; Na, W.; Yang, H.; Cho, K. H.; Lee, S. H.; Song, H. S.; Jang, J.; Park, T. H. High-performance bioelectronic tongue using ligand binding domain T1R1 VFT for umami taste detection. *Biosensors and Bioelectronics* **2018**, *117*, 628–636.

(51) Wei, X.; Qin, C.; Gu, C.; He, C.; Yuan, Q.; Liu, M.; Zhuang, L.; Wan, H.; Wang, P. A novel bionic in vitro bioelectronic tongue based on cardiomyocytes and microelectrode array for bitter and umami detection. *Biosensors and Bioelectronics* **2019**, *145*, 111673.

(52) Dang, Y.; Hao, L.; Zhou, T.; Cao, J.; Sun, Y.; Pan, D. Establishment of new assessment method for the synergistic effect between umami peptides and monosodium glutamate using electronic tongue. *Food Research International* **2019**, *121*, 20–27.

(53) Wang, W.; Zhou, X.; Liu, Y. Characterization and evaluation of umami taste: A review. *TrAC Trends in Analytical Chemistry* **2020**, *127*, 115876.

(54) Hwang, Y.-H.; Ismail, I.; Joo, S.-T. Identification of Umami Taste in Sous-Vide Beef by Chemical Analyses, Equivalent Umami Concentration, and Electronic Tongue System. **2020**, *9*.

(55) Fukushima, K. L.; Scagion, V. P.; Facure, M. H. M.; Pinheiro, A. C. M.; Correa, D. S.; Nunes, C. A.; Oliveira, J. E. Development of an Electronic Tongue Based on a Nanocomposite for Discriminating Flavor Enhancers and Commercial Salts. *IEEE Sensors Journal* **2021**, *21*, 1250–1256.

(56) Paulovich, F. V.; Moraes, M. L.; Maki, R. M.; Ferreira, M.; Oliveira Jr., O. N.; de Oliveira, M. C. F. Information visualization techniques for sensing and biosensing. *Analyst* **2011**, *136*, 1344–1350.

(57) Srivastava, A. K.; Dev, A.; Karmakar, S. Nanosensors and nanobiosensors in food and agriculture. *Environmental Chemistry Letters* **2018**, *16*, 161–182.

(58) Smyth, H.; Cozzolino, D. Instrumental Methods (Spectroscopy, Electronic Nose, and Tongue) As Tools To Predict Taste and Aroma in Beverages: Advantages and Limitations. *Chemical Reviews* **2013**, *113*, 1429–1440.

Graphical TOC Entry

Some journals require a graphical entry for the Table of Contents. This should be laid out "print ready" so that the sizing of the text is correct.
Inside the `tocentry` environment, the font used is Helvetica 8 pt, as required by *Journal of the American Chemical Society*.
The surrounding frame is 9 cm by 3.5 cm, which is the maximum permitted for *Journal of the American Chemical Society* graphical table of content entries. The box will not resize if the content is too big: instead it will overflow the edge of the box.
This box and the associated title will always be printed on a separate page at the end of the document.